Equilibrium and glassy states of the Asakura-Oosawa and binary hard sphere mixtures: Effective fluid approach

Ph. Germain and S. Amokrane
Physique des Liquides et Milieux Complexes, Faculté des Sciences et Technologie, Université Paris XII, Val de Marne, 61 Avenue du Général de Gaulle, 94010 Créteil Cedex, France
(Received 29 March 2007; published 13 September 2007)

Motivated by recent experimental results on model binary colloidal mixtures, especially for the glass transition, we investigate the phase diagram of two models of asymmetric binary mixtures: the hard sphere and the Asakura-Oosawa mixtures. This includes the binodals and the glass transition line, computed in the effective one-component representation using the corresponding potentials of mean force at infinite dilution. The reference hypernetted chain approximation is used for computing the static properties and the glass transition line is computed in the mode coupling approximation. The similarities and the differences between the two models are discussed for different size ratios. It is shown that while both models follow a universal behavior at large asymmetry, the hard sphere mixture model leads to more original results at moderate size ratio. These results show that a modeling beyond generic effective potentials might be necessary for an appropriate description of the complete phase diagram.

DOI: 10.1103/PhysRevE.76.031401 PACS number(s): 82.70.Dd, 64.60.−i, 05.20.Jj

I. INTRODUCTION

Understanding the macroscopic properties of colloidal suspensions from a microscopic point of view is important both for fundamental aspects in condensed matter physics and for practical applications. On the one hand, the possibility to tune the interaction potential between colloidal particles and their coupling with external fields allows us to use colloids as convenient model systems for studying a variety of phenomena, such as, for example, crystal nucleation, glass transitions, solid-solid ones, etc., that are more difficult or even impossible to investigate with atomic or molecular materials (see, e.g., [1]). On the other hand, an analysis at the microscopic level can be very useful for practical purposes. One may, for example, try to predict in this way the precise physico-chemical parameters that govern the rheology or the phase behavior of the suspension. To take, for illustration, the specific situation of protein crystallization, one may be interested in the precise conditions that would favor the crystal with respect to the gel (see [2,3], and references therein).

It is, however, clear that a theoretical study that would incorporate a detailed description of a real suspension would first be a very difficult technical task. Furthermore, given the great diversity of phenomena observed when varying the various physico-chemical parameters, this might obscure common fundamental mechanisms. It is then better to start with simpler models that capture the basic characteristics of such a complex system, the most obvious one being the large difference in size between the particles. This was done in the model introduced by Asakura-Oosawa (AO) [4] and Vrij [5] for studying the depletion forces in colloid-polymer mixtures. In this so-called Asakura-Oosawa mixture model, the small particles (polymers) behave as an ideal gas but they experience a hard-core repulsion with the big hard spheres (the colloids). In other words, the big-big and big-small interactions are hard-sphere (HS) ones, but the small-small interactions vanish. This model is thus characterized by the colloid-polymer diameter ratio $q=\sigma_b/\sigma_s>1$ [with σ_b the hard-core diameter of the colloids, σ_s that of the polymers; the radius of the exclusion sphere is $\sigma_{bs}=\frac{1}{2}(\sigma_b+\sigma_s)$]. A second simple model is the binary HS mixture, in which all the interactions (big-big, big-small, and small-small) are modeled by the HS potential. For convenience, this model will be referred to in this paper as the "HS model" which stands for "HS mixture model." In both models, the composition is characterized by the packing fractions $\eta_i=\frac{\pi}{6}\rho_i\sigma_i^3$, $i=s,b$ (where ρ_i is the number density).

Since the early work of Asakura and Oosawa, these models have been the subject of numerous studies (see, for example, references in [6–21] for analytical methods and [22–27] for simulations). This continued interest is motivated by the fact that not only may one address from these very simple models fundamental questions such as the purely "entropic" phase transitions, the validity of the effective fluid approach, etc., but they may also be useful to analyze the behavior of colloid-polymer mixtures (AO model) or pseudobinary mixtures of hard-sphere-like colloids (HS mixture) [28–31]. Indeed, in the literature, these models are not presently viewed as two approximate representations of the same reality, but rather as models for actually different physical systems. Although their limitations for describing real suspensions have already been emphasized (see, e.g., [32,33]), they are still frequently used for discussing the generic effects in colloidal suspensions. As far as the binodals in the phase diagram are concerned, several theoretical studies have established a rather consistent picture. These lines that locate the boundaries of the thermodynamic equilibrium states share some general characteristics at large asymmetry. They are conveniently discussed in the effective one-component fluid (EOCF) representation, which describes a fluid of big particles interacting through the potential of mean force at infinite dilution. For the AO (respectively, HS) model, the effective potential will be called "AO depletion

potential" (respectively, "HS depletion potential"). The variables are then the packing fraction of the big spheres, η_b, and that of the small particles in the reservoir, η_s^*. In this representation, one observes for both depletion potentials a fluid-solid (FS) coexistence domain which broadens very rapidly when η_s^* increases. No stable fluid-fluid (FF) binodal is observed at large asymmetry. These features are a consequence of the fact that the depletion potential is both very short ranged and very deep at contact (a stable solid-solid isostructural transition is also observed for $q>10$, as in simple fluids with very short-range attractions (see, for example, [34,35]). There exists, however, an important difference between the result found with the AO and HS depletion potentials concerning the FF transition at moderate asymmetry. For the HS depletion potential, this transition is found only for $q \geqslant 10$ (and it is metastable), while it is systematically present for the AO one. In the latter case, it has a stable part for $q \leqslant 3$.

Therefore, while the results found for the AO depletion potential are typical of those obtained for standard potentials having a hard core and an attractive part (e.g., Yukawa or square-well potentials), the HS depletion potential leads to a more specific behavior. This means that the gross trends deduced from generic models of the effective interactions have to be taken with care when describing the thermodynamics of these mixtures. One of the motivations of this paper is to further discuss this point, by considering the full phase diagram, including the glass transition.

A complete description of the phase behavior requires the determination of those states with particular dynamic properties such as the glassy states [36], besides the boundaries of the stable and metastable domains. These properties can indeed affect the occurrence of the equilibrium phase transitions (for a review, see, for example, [37]). Recent experimental studies on colloid-polymer mixtures have evidenced two distinct glassy states [38–44]. At low η_s, the glassy state is that of the one-component fluid of big hard spheres. It exists only in the dense fluid region [45–47]. It is due to the "caging" effect experienced by each big particle in a dense disordered state ("repulsive glass": see [36,47–50]). At greater η_s, the glass transition is shifted to lower values of η_b. The corresponding glassy state, which exhibits different dynamical properties (see, e.g., [41,42,44]), is attributed in the theoretical analysis to the depletion attraction between the big particles, which allows their connection in loose packed structures ([43], and references therein). This view ("attractive glass") is substantiated by mode coupling calculations [2,51–54] and simulations [55,56]. These studies have indeed shown that such low density glasses exist for sufficiently short attraction range. However, very few results [40,57,58] exist for explicit models of the mixture.

We will thus present in this paper the complete phase diagram (binodals and glass transition) of two models: the AO mixture and the HS mixture, *both treated in the EOCF representation*. Our first motivation is that the glass transition has not yet been determined theoretically for the HS mixture (neither from a true mixture theory nor from the EOCF with the HS depletion potential) and it has been obtained only for limited situations [40,57] for the AO mixture. On the other hand, as recalled above for the binodals (see also [32,33]), one should be careful, when extrapolating the trends relative to "generic" potentials, also for the glass transitions. Indeed, the dependence of the depletion potential on the physical parameters, the density and the size ratio here, is more complex than what can be reproduced with these generic models such as the square well or the Yukawa potential. The second motivation of this paper is precisely to investigate this question. We will show that, contrarily to a view often present in the literature (see, however, [59] for fullerene) a proper account of this dependence is in fact necessary, even in the simplest situations discussed above (HS and AO mixtures).

This paper is hence organized as follows: In Sec. II, we summarize the theoretical methods used for computing the phase diagram in the EOCF. These methods are checked by comparison with existing data. In Sec. III, the phase diagrams computed for the AO and HS depletion potentials are discussed for two different size ratios. The features observed are interpreted by the specificities of the depletion potential relative to each model. Section IV is the conclusion.

II. THEORETICAL METHODS

A. One-component fluid representation

The theoretical description of a highly asymmetric binary mixture in terms of a one-component fluid of big particles interacting through the potential of mean force mediated by the small ones, computed at infinite dilution, is well known [60]. We briefly recall it here by using the notations of recent literature [the reader may switch directly to Eq. (7)].

The convenient statistical ensemble is in this case the semi-grand one with state variable $(N_b, V, T; \mu_s)$ where N_b is the number of big particles, V the volume, T the temperature, and μ_s the chemical potential of the small particles. One may view it as describing an osmotic equilibrium system in which the mixture is in contact with a reservoir of small particles having the chemical potential μ_s. The EOC representation is formally defined from the semi-grand free energy $F(N_b, V, T; \mu_s)$

$$\beta F = -Ln\left(\mathrm{Tr}_{b,N_b}\left[\sum_{N_s}^{\infty} \mathrm{Tr}_{s,N_s}[\exp(-\beta(H-\mu_s N_s))]\right]\right), \tag{1}$$

where $H=H_{bb}+H_{sb}+H_{ss}$ is the total interaction potential of the mixture (with H_{ij} the total interaction potential between species i and j), $\beta=1/k_B T$ (with k_B Boltzmann's constant), and where the operator $\mathrm{Tr}_{\alpha,N\alpha}$ is defined by

$$\mathrm{Tr}_{\alpha,N_\alpha}[X] = \frac{1}{N_\alpha! \Lambda_\alpha^{3N_\alpha}} \int \left(\prod_{i=1}^{N_\alpha} dr_i\right) X(r_1, \ldots, r_{N_\alpha}), \tag{2}$$

with

$$\Lambda_\alpha = h/\sqrt{2\pi m_\alpha k_B T}. \tag{3}$$

F may also be written as

$$\beta F = -Ln[\mathrm{Tr}_{b,N_b} \exp(-\beta H^{\mathrm{eff}})] \tag{4}$$

where

$$\exp(-\beta H^{\mathrm{eff}}) = \sum_{N_s=1}^{\infty} \mathrm{Tr}_{s,N_s}[\exp(-\beta(H-\mu_s N_s))]. \tag{5}$$

From Eqs. (4) and (5), which are exact, F appears as the free energy of an EOCF with an interaction Hamiltonian $H^{\mathrm{eff}} = H_{bb} + H^{\mathrm{ind}}$ where H^{ind} is defined by

$$\beta H^{\mathrm{ind}} = -Ln\left\{\sum_{N_s=1}^{\infty} \mathrm{Tr}_{s,N_s}[\exp(-\beta(H_{ss}+H_{sb}-\mu_s N_s))]\right\}. \tag{6}$$

H^{ind} is the indirect part of the interaction between the big particles that is mediated by the small ones. It is in general a function of the positions of the N_b big particles that cannot be reduced to a sum of pair interactions. The standard approximation in the study of highly asymmetric mixtures consists in replacing the potential of mean force H^{ind} by a sum of two-body contributions computed for a pair of macroparticles at infinite dilution in the pure fluid of small particles ([12], third paper). The part H' of H^{eff} that is relevant for the phase transitions of the EOCF is then a pair additive interaction:

$$H' = \sum_{i<j} [u_{bb}(r_{ij}) + \phi^{\mathrm{eff}}(r_{ij})], \tag{7}$$

where u_{bb} is direct interaction between the big particle and ϕ^{eff} the indirect one. The latter can be obtained from the infinite dilution limit of the pair distribution function (pdf), of the big particles, g_{bb} [60,61]:

$$\phi^{\mathrm{eff}}(r,\mu_s) = -k_B T\, Ln(g_{bb}(r,\rho_b \to 0)) - u_{bb}(r). \tag{8}$$

In practice, however, the convenient variables are the densities rather than the chemical potentials. The thermodynamic state of the pure fluid of small spheres in the reservoir is then characterized by its reduced density ρ_s^* (in units of σ_s^3) rather than by μ_s. At fixed T, μ_s is associated with a unique value of ρ_s^*, in the one-phase domain. This holds for the HS fluid before the freezing density, as assumed here (the temperature is irrelevant for the two models considered here). Both variables being then strictly equivalent in Eq. (8), the phase diagram is most conveniently computed in the (ρ_s^*, η_b) plane.

The accuracy of this reduction to the effective fluid depends on the validity of the pair interaction approximation. For sufficiently asymmetric HS mixtures, accounting only for the two-body effects is sufficient for computing $g_{bb}(r,\rho_b \neq 0)$ [26] for the range of asymmetry considered in this paper, at least in the conditions accessible to simulations. Unexpectedly, this holds down to $q=3.33$ (second paper in Ref. [26]). Furthermore, the EOCF binodals computed in several studies (see, for example, [12,13,16]) are consistent with existing simulation data for the true mixture [12], that is at low packing fraction of the small spheres. More recently, the equivalence of both representations up to the dense fluid region for the small particles (typically $\eta_s=0.4$) has been established by using integral equations [21]. For sufficiently asymmetric AO mixtures, the validity of the pair approximation is more easily established due to the absence of interaction between the small particles. It becomes even exact for $\frac{\sigma_s}{\sigma_b} < \frac{2}{3}\sqrt{3}-1$ $(q>6.46)$ since contributions beyond two-body terms to H^{eff} vanish then (see, e.g., [15,18,13]).

The pair potential of mean force $\phi_{\mathrm{HS}}^{\mathrm{eff}}$ for binary HS mixtures (that is the HS depletion potential) can be computed by different methods (see, for example, references in [62]). We briefly recall here the method employed in our group: the effective potential is computed from Eq. (8). The pdf's $g_{ij}(r)$ for a mixture with $\rho_b \to 0$ are computed from the Ornstein-Zernike equations (OZE) [61] with the reference hypernetted-chain (RHNC) closure [63]. The bridge functions are computed from Rosenfeld's density functional theory [64] in the limit $\rho_b \to 0$. The accuracy of this method which can be generalized to non-HS interaction potentials [65] has been positively checked against the simulation data of Refs. [66,67]. It also proved to be accurate even in situations including extremely short-range attractions [33].

For the AO mixture, the potential of mean force at infinite dilution (AO depletion potential) has the well-known exact expression (in units of $k_B T$)

$$\phi_{\mathrm{AO}}(x) = \begin{cases} \infty, & x<1 \\ -\frac{\pi}{4}q^3\rho_s^*\left[\frac{2}{3}\left(1+\frac{1}{q}\right)^3 - x\left(1+\frac{1}{q}\right)^2 + \frac{x^3}{3}\right], & 1 \leqslant x \leqslant 1+\frac{1}{q} \\ 0, & x > 1+\frac{1}{q}, \end{cases} \tag{9}$$

in which x is the interparticle distance in units of the big spheres' diameter σ_b [4,5]. As a generic model for the effective interaction, we will also consider at the end of this section the attractive hard-core Yukawa potential:

$$\phi_{\mathrm{Yuk}}(x>1) = -\frac{\varepsilon^*}{x}\exp\{-\kappa^*(x-1)\},$$

$$\phi_{\mathrm{Yuk}}(x\leqslant 1) = +\infty, \tag{10}$$

whose depth (in units of k_BT) and range (in units of the hard-core diameter) are controlled by the dimensionless parameters ε^* and κ^*.

B. Binodals

The binodals are obtained in the (ρ_s^*, η_b) plane by computing the EOCF free energy as a function of η_b, the effective potential $\phi^{\mathrm{eff}}(r,\rho_s^*)$ being computed for a series of small particle densities ρ_s^* in the reservoir as indicated above. For the fluid phase, the very accurate RHNC integral equations [63] were used with the bridge function of Malijevski and Labik [68] as unique input (see Ref. [69] for details). The free energy of the solid was computed in the variational perturbation theory described in [35]. The accuracy of this hybrid method that computes the fluid and solid free energy following two distinct routes was shown in Ref. [16] for the FS and FF transitions, by comparison with the simulation data of Dijkstra *et al.* [12], and confirmed by simulations from our group [67] for the FF transition. As already mentioned, these results are also consistent with those obtained from a theory for the true mixture [21]. Note that concerning the FS transition (but not the FF one), it would be acceptable to apply the same perturbation treatment to both the fluid and solid free energies [69].

Concerning the FF transition, one important limitation of integral equations is the existence of a nonconvergence region that crosses the FF binodal [for the true mixture, this problem is solved [21] by using the special ("RHNC-MSA") closure introduced in [27]]. For short-range attractive hard spheres, however, a rather precise location of the FF line is generally feasible because the latter is almost horizontal in the (ρ_s^*, η_b) representation, making easier the extrapolation in the nonconvergence region. When more points were necessary in the very dilute region ($\eta_b \leqslant 0.07$), we used a second order virial expansion that we checked positively very close to the no-solution domain.

Concerning solid-solid transitions it was shown in [69] that the perturbation theory allows only a qualitative description (it was encountered in one of the situations we investigated). Indeed, although this method is suitable to describe a dense solid near close packing, it cannot be extended safely to a "softer" one with lower density. However, the transition found here is consistent with the MC simulation of Ref. [12].

C. Glass transition

The glassy state has the same static properties and microstructure as the fluid. It is a dynamically arrested state, which can be defined by the onset of a nonvanishing long time limit of the particle density autocorrelation function (dynamical arrest) in place of the usual exponential decay of the nonglassy fluid. In the recent years, one of the most popular methods used to study the glass transition, especially in the context of colloids, is the mode coupling approximation (MCA) [36]. We will consider here its formulation for the EOCF representation. The general procedure is briefly recalled below [it is possible to go directly to Eqs. (15) and (14), from which the glass transition line is computed, with the help of the definition (11)].

For colloids in a continuous solvent, the starting point is the Smoluchowski equation that describes the time evolution of the N-particle configuration probability (this also holds for a treatment by Brownian dynamics) [70]. It is a coarse grained equation which is deduced from the N-particle Langevin equations in the overdamped regime, by integrating out first the degrees of freedom relative to the random force due to the solvent, second those relative to the particle velocities. This procedure, whose justification is based on the comparison of the involved relaxation times, leads to the Smoluchowski equation that contains information only on the particle coordinates. This equation is analogous for colloidal systems of the Liouville equation for molecular systems. The projection operator formalism is then used in the MCA to describe the evolution of the dynamic functions. For colloids ([71,72], and references therein), the principal difference with molecular fluids is that only one hydrodynamic mode, the density one, is relevant in the MCA because the current fluctuations are damped instantaneously by viscous forces at the scale of the coarse grained time. By neglecting further the hydrodynamic interactions, the density autocorrelation function $\phi_q(t)$, defined as

$$\phi_q(t) = \frac{\langle \rho_{\mathbf{q}}^*(t)\rho_{-\mathbf{q}}(0)\rangle}{\langle \rho_{\mathbf{q}}^*(0)\rho_{-\mathbf{q}}(0)\rangle}, \tag{11}$$

with $\rho_{\mathbf{q}}(t)=\Sigma_{j=1}^{N_b}\exp(-i\mathbf{q}\cdot\mathbf{R}_j)$, is given in the MCA by a nonlinear integro-differential equation:

$$\dot{\phi}_q(t) + q^2 D_0\left\{\phi_q(t) + \int_0^t m_q(t-t')\dot{\phi}_q(t')\right\} = 0. \tag{12}$$

In Eq. (12), D_0 is the single particle diffusion constant, and $m_q(t)$ the memory function:

$$m_q(t) = \frac{1}{2}\int \frac{d^3k}{(2\pi)^3} V(q,k)\phi_k(t)\phi_{|\mathbf{q}-\mathbf{k}|}(t), \tag{13}$$

where

$$V(q,k) = -\frac{\rho_b}{q^4}\{\mathbf{q}\cdot(\mathbf{q}-\mathbf{k})c_{|\mathbf{q}-\mathbf{k}|} + \mathbf{q}\cdot\mathbf{k}c_k\}^2 S_q S_k S_{|\mathbf{q}-\mathbf{k}|}, \tag{14}$$

where c_k is the static direct correlation function and $S_k = \frac{1}{1-\rho_b c_k}$ the static structure factor (this expression neglects the contribution from three-body direct correlations). $\phi_q(t)$ can thus be computed from Eqs. (11)–(14), using c_k as unique input. The determination of the glass transition line requires only the long time limit $f_q = \phi_q(t\to\infty)$, since the dynamical

arrest is defined by $f_q \neq 0$. It can be shown from the mathematical study of Eqs. (11)–(13) [73] that f_q is the greatest solution [48,36] in the range $0 \leqslant f_q \leqslant 1$ of the equation

$$\frac{f_q}{1-f_q} = \frac{1}{2}\int \frac{d^3k}{(2\pi)^3} V(\mathbf{q},\mathbf{k}) f_k f_{|\mathbf{q}-\mathbf{k}|}. \tag{15}$$

This solution is in fact the limit of the direct iterative process defined by $f_q^{(0)}=1$, $f_q^{(n+1)}=\frac{m_q(f_q^{(n)})}{1+m_q(f_q^{(n)})}$ where $m_q(f_q^{(n)}) = \frac{1}{2}\int \frac{d^3k}{(2\pi)^3} V(\mathbf{q},\mathbf{k}) f_k f_{|\mathbf{q}-\mathbf{k}|}$ is the long time limit of Eq. (12) [73]. The glass transition lines shown in this paper have been computed following this route. To obtain the input EOCF static direct correlation functions, we used the RHNC integral equation.

The MCA has been widely employed to study the properties of the glassy states for one-component HS fluids [47–50] and for HS ones with attractive forces ([51–53,37]). For HS fluids, the transition lines computed from the MCA are shifted with respect to simulation data [55]: one finds $\eta_{\text{glass}}=0.525$ in the MCA [36] and $\eta_{\text{glass}}=0.582$ from simulations. Furthermore, in the experimental suspension studied in [47] of supposedly HS-like colloids, the glass transition was found for $\eta_{\text{glass}}=0.58$. A significant uncertainty exists thus for the precise location of the glass transition line, the MCA certainly overestimating the glassy state region. However, a much better agreement between theory and simulations exists [55] concerning the *variations* of η_{glass} induced by short-range attractive tails added to the HS potential. We do not aim in this work at a precise determination of the glass transition line, but at discussing the influence of the form of the interaction potential within the same theory. The trends discussed below, and obtained from our MCA treatment, should thus be valid.

Another question is the use of the effective fluid representation. Using the EOCF approximation to describe the glass transition in sufficiently asymmetric mixtures is based on the view that the dynamical arrest involves essentially the fluid of big particles. The small particles that move "freely" in the free volume left by the network of big ones are merely responsible for the attractive part of the effective interaction $\phi^{\text{eff}}(r,\rho_s^*)$. This view has been partly checked against Brownian dynamics simulations in [57] for an AO mixture in the low ρ_s region: the MCA glass transition lines ($q^{-1}=0.15,0.5$) were computed both for the EOCF and the two-component fluid. Brownian dynamics isodiffusivity lines were computed for two extreme values of the short-time mobility ratio $\alpha=\sqrt{m_s/m_b}$: $\alpha=1,0.01$. The EOC version of the MCA proved to reproduce correctly the trends obtained by simulations for $\alpha=0.01$, while the two-component version was appropriate for $\alpha=1$. This result is consistent with the adiabadicity criterion established in [74] that requires a minimum number of collisions during the time for a big particle to move along a distance σ_s, a scale typical of the indirect interaction. This also confirms the intuitive view that the EOC representation should be more suitable at large asymmetry. Clarifying this point would, however, require a deeper analysis, since the relation between α and the size of the particles depends on the system under study: for a mixture of two differently sized hard colloids (with $m_i \approx \sigma_i^3$) for example, one would expect α to behave roughly as $\alpha \approx q^{-3/2}$, while for colloid-ideal polymer mixtures, the dependence is more complex. Let us just mention that, for a mixture of HS with the same mass density, the criterion proposed in [74] is satisfied for small particle packing fractions $\eta_s \geqslant 0.065$ for $q=4$, and $\eta_s \geqslant 0.0012$ for $q=12.5$, the two size ratios investigated here. The question of the gelation of the fluid of small particles arises, however, when their density is sufficiently high. This is suggested by some experiments on HS-like colloids [30] and simulations [75], on systems with an additional soft repulsion, however.

D. Test of the method

For hard spheres with short-range attractive interactions, the accuracy of the method employed for computing the static quantities is essential both for the binodals and for the glass transition lines: we know for example that the mean spherical (MSA) or Percus-Yevick (PY) approximations predict critical temperatures of the Yukawa fluid that strongly differ from those of more accurate integral equations, such as the self-consistent Ornstein-Zernike approximation (SCOZA) [2] or the RHNC. Similar observations can be made for the glass transition line found with SCOZA [2] and with MSA [51]. As the MCA glass transition line has not yet been determined with RHNC static input, we first tested this method (also for the binodals) for the very short-range attractive Yukawa potential studied in [2], and for two asymmetric AO mixtures at low solvent density studied in [40,57].

1. Yukawa potential

We computed the phase diagram for a Yukawa potential with reduced inverse range $\kappa^*=30$ (Fig. 1) using the RHNC/MCA method described above. For this value, results are available from MSA [51] and SCOZA [2]. For this value the SCOZA glass transition line passes through the metastable liquid-gas critical point. The FS transition lines found here are almost identical to the SCOZA ones. For the FF transition, only the spinodal was computed in [2]. Our binodal is close to this line. The critical points can be compared since it is the point where the binodal and the spinodal have a common point. We find $T_c^{\text{RHNC}} \approx 0.24$ to be compared with $T_c^{\text{SCOZA}} \approx 0.22$. As already mentioned, these values differ strongly from the MSA or PYA ones since one has roughly $T_c^{\text{MSA,PYA}} \approx 0.5\ T_c^{\text{SCOZA,RHNC}}$.

The agreement between the RHNC and SCOZA predictions for the glass transition is also good. At infinite temperature, we find $\eta_{\text{glass,HS}}=0.526$ (the three digits given here as the result of the MCA calculation should not be taken literally). When decreasing the temperature, the expected decrease of η_{glass} is observed, our transition line being slightly above the SCOZA one (we get, for example, $\eta_{\text{glass}}=0.2$ for $T^*=0.26$ instead of $T^*=0.22$ in [2]). The region of the FS coexistence domain for which the system is expected to gelate is thus more extended. The value of κ^* for which the glass transition crosses the FF critical point is also a bit smaller. Like for the binodals, these discrepancies are, however, small by comparison with those found with the MSA

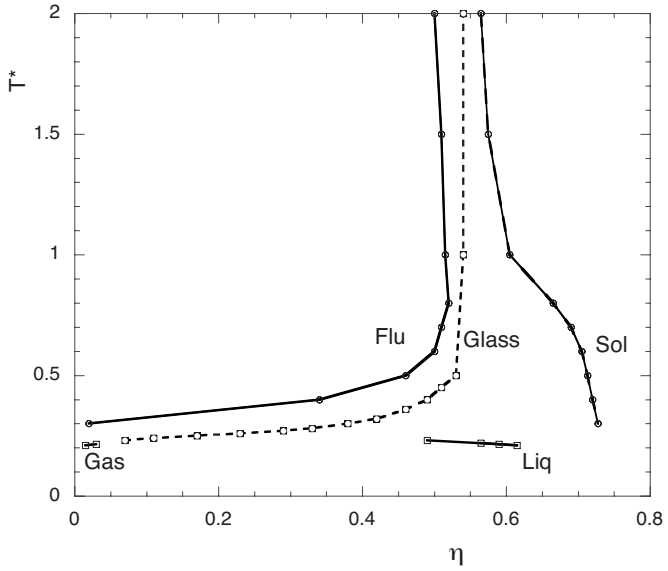

FIG. 1. Phase diagram of the Yukawa one-component fluid with reduced inverse range $\kappa^*=30$ in the packing fraction (η)–reduced temperature (T^*) plane computed with the RHNC/MCA method described in Sec. II. Solid lines, binodals; dashes, glass transition line. The lines connect the state points (symbols) for which the calculations have actually been done.

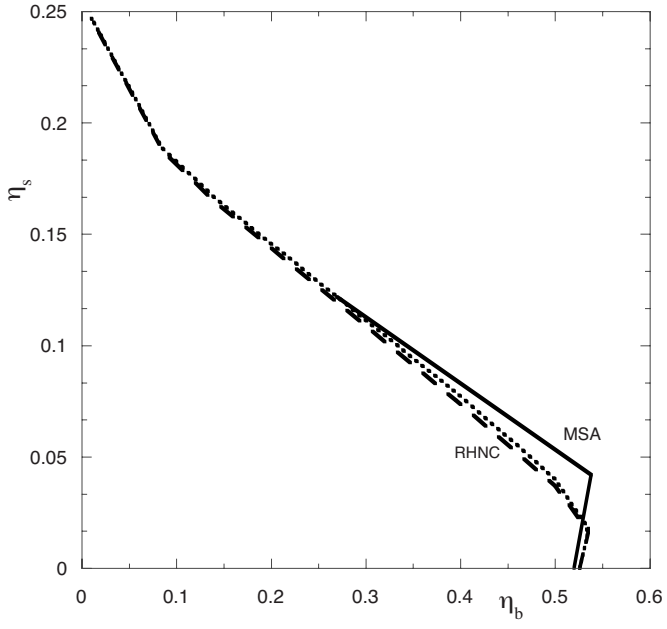

FIG. 2. Glass transition line of the Asakura-Oosawa model, for $q=12.5$, in the big (η_b)-small (η_s) particle packing fraction plane. The solid line, computed from the MSA static input, is extracted from Ref. [40]. The dashed and dotted lines are deduced from the glass transition line of the EOCF, computed from RHNC input, by using Eq. (A14) of the Appendix. For each value of η_b, the actual value of η_s lies between these two lines.

and PYA inputs. These results confirm thus that while the simple MSA or the PYA approximations are sufficient for pure hard spheres, more accurate integral equations are necessary for computing the FF binodal and the glass transition line of short-range attractive hard spheres.

2. Asakura-Oosawa model at small ρ_s

We next computed the MCA glass transition line for an AO mixture with $q=12.5$ at low density ρ_s of the small particles in the mixture ($\eta_s<0.25$; Fig. 2). The same calculation with MSA input has been done in [40] in a two-component mixture theory (for $\eta_s<0.122$), for analyzing the experimental behavior of a mixture of polymethylmethacrylato particles and nonadsorbing polystyrene. Since we used here the EOCF representation, the comparison was done with the conversion relation $\rho_s=\rho_s^*\left(1-\frac{4\pi\rho_b\sigma_{sb}^3}{3}\right)$. A more precise analysis of this approximation, known to be reasonable for $q\gg 1$, is given in the Appendix. For $q=12.5$, the effect of this approximation is not observable in the density range studied (see Fig. 2). The trends we find are similar to those of [40] after deduction of their *ad hoc* scaling: both transition lines show a reentrant behavior for η_b slightly above the HS critical value $\eta_{b,\mathrm{HS}}^g=0.525$. This reentrance is, however, notably weaker with the RHNC input than with the MSA one. Note that the shift $\Delta\eta_b^g=\eta_{b\ \max}^g-\eta_{b\mathrm{HS}}^g$ between the maximum value of η_b^g and that of the HS fluid is independent of the representation used (EOC versus mixture).

We also did the same calculation, still for the AO model, for $q^{-1}=0.15$. For this value the glass transition line was computed, in a two-component mixture theory, for $\eta_s<0.08$ in [57] using static structure factors deduced from the fundamental measure density functional theory [76]. A detailed comparison with our EOCF results is, however, more difficult, because the uncertainty on ρ_s induced by the approximation described above is significant for $q^{-1}=0.15$. Our results are, however, qualitatively consistent with those of [57]. In particular, the reentrant behavior is also observed. Note also that a reentrant behavior is also suggested for a polymer colloid mixture treated in the polymer reference interaction site model/ Percus-Yevick closure in Ref. [58] (a simple criterion was used for the glass transition).

III. RESULTS

In this section we present the binodals and the glass transition lines in the effective one-component fluid representation for the AO and the HS depletion potentials. The size ratios investigated are $q=4$ and $q=12.5$. The aim is to analyze the respective influence of the size asymmetry—a generic characteristic of colloids—and that of more specific features of the model with a view to assessing the extent to which the results obtained with generic potentials (like the Yukawa potential) can be extrapolated to actual mixtures. A crude correspondence can be made between the AO and the Yukawa fluid by equating the values of the respective interaction potential and of the slope at contact. One gets $\kappa^*=\frac{2(q^2-1)}{q+2/3}$. This leads to $\kappa^*=6.7$ (moderately short range) for $q=4$, and $\kappa^*=23.7$ for $q=12.5$ (very short range). This corresponds thus—*a priori*—to the two distinct situations described in the literature, concerning either the glass transition (existence or not of an attractive glass, competition with the

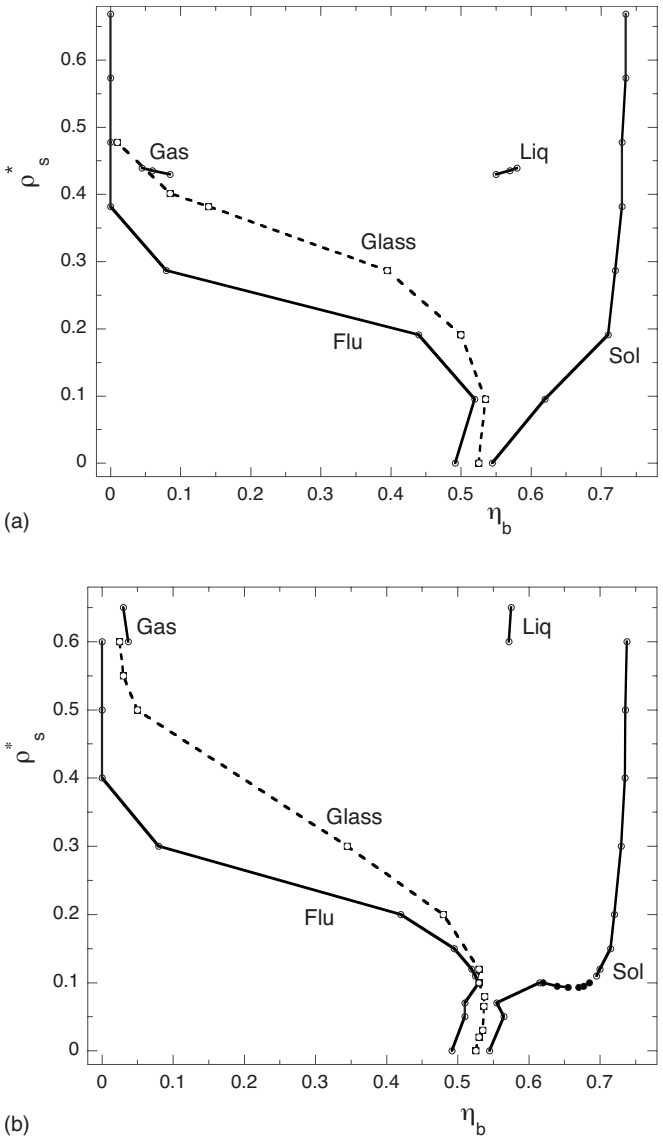

FIG. 3. Phase diagram of the Asakura (a) and HS mixture (b) models for $q=12.5$ in the EOCF representation. Solid lines, binodals; dashes, glass transition lines. (b) The filled circles locate the solid-solid transition.

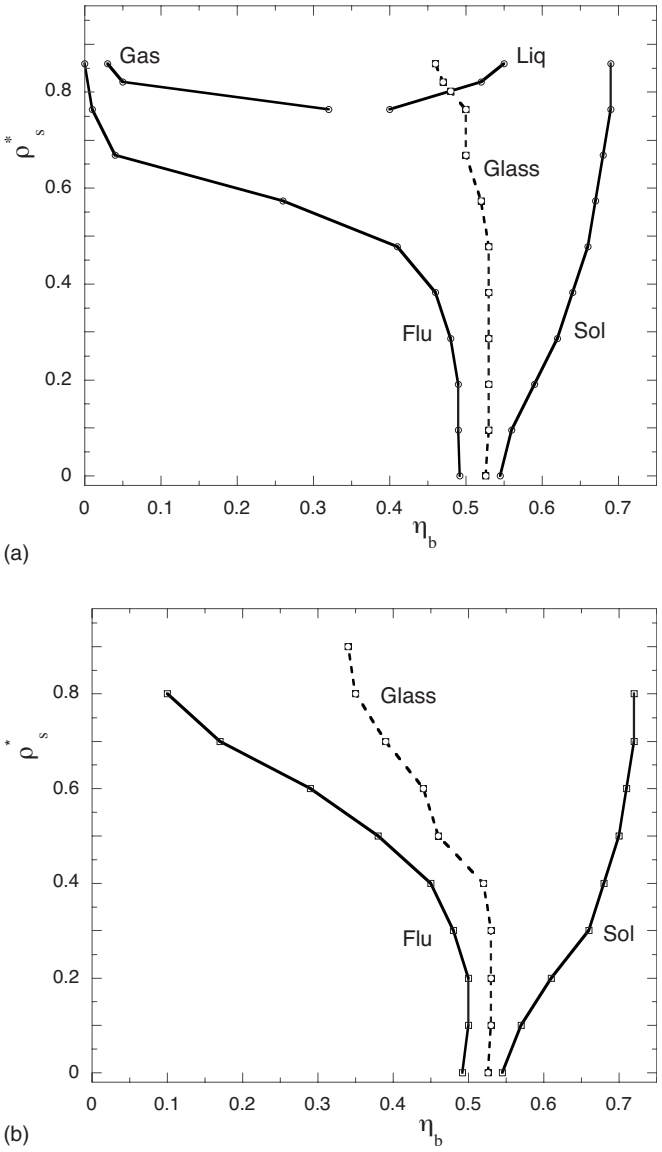

FIG. 4. Same as Fig. 3 for $q=4$. For hard spheres (b), neither the FF nor the SS transition is observed.

FF transition) or the equilibrium states (stability of the homogenous fluid, location of the FF binodal). The results presented here investigate this issue.

A. Phase diagrams for $q=12.5$ and $q=4$

The complete phase diagrams computed for the AO and HS depletion potentials are shown in Figs. 3 ($q=12.5$) and 4 ($q=4$).

1. q=12.5

The two phase diagrams exhibit many similarities, which aside from slight differences correspond to the features expected for very short-range attractive HS: (i) The abrupt widening of the FS coexistence domain when ρ_s^* increases and taking place here for $\rho_s^* \approx 0.2-0.30$. (ii) The instability of the FF binodal, which is clearly preempted by the FS one. This is even more marked with $\phi_{\mathrm{HS}}^{\mathrm{eff}}$ (FF critical density $\rho_s^{*c}=0.55$) than with ϕ_{AO} ($\rho_s^{*c}=0.41$) (for $\phi_{\mathrm{HS}}^{\mathrm{eff}}$ the value of ρ_s^{*c} can be estimated precisely from the free energy curves but the corresponding η_b is not accessible—see Fig. 3(b)—because of the nonconvergence problem). (iii) The flatness of the FF binodal (note also that for the HS mixture, however, a narrow homogeneous fluid region exists at high ρ_s^*). (iv) The preemption of the FF transition by the glass transition. This is, however, slightly incomplete at low η_b for the AO fluid, for which the binodal occurs at lower ρ_s^* than for pure HS. For both models, the glass transition line is located inside the FS coexistence domain. (v) The SS isostructural transition. It is stable only for $\phi_{\mathrm{HS}}^{\mathrm{eff}}$, its stability domain being very narrow. This result is consistent with those of Ref. [12], for HS mixtures with $q=10,20$ (in that study, the critical point of the SS transition is stable for $q=20$, and metastable for $q=10$ but very close to the FS binodal). Note also that a reentrance of

the fluid phase seems to occur at low ρ_s^* but we did not investigate this point further.

2. q=4

At this size ratio, the phase behaviors of the two models show significant differences, both for the binodals and the glass transition. Concerning the FF binodal, several studies exist in the literature for similar size ratios. The general pattern is as follows: a FF binodal is observed only for the ϕ_{AO}, with a critical solvent packing fraction in the reservoir $\rho_s^{*c} \approx 0.76$. It is metastable with respect to the FS one. For $\phi_{\mathrm{HS}}^{\mathrm{eff}}$, no FF transition is observed. The HS and AO FS binodals show similar behavior at low ρ_s^*. A more significant difference is observable on the freezing line at higher ρ_s^*: it is flatter and closer to the left axis for ϕ_{AO}. Concerning the glass transition for $\rho_s^* \leqslant 0.8$ (see below for greater ρ_s^*), the glassy state domain is confined for ϕ_{AO} to the very dense fluid region, $\eta_b^{\mathrm{glass}} \geqslant 0.50$, close to the value for pure hard spheres, the transition line being nearly vertical. In contrast, with $\phi_{\mathrm{HS}}^{\mathrm{eff}}$, η_b^{glass} decreases when ρ_s^* increases beyond $\rho_s^* \approx 0.4$, eventually dropping much below the HS value (say $\eta_b^{\mathrm{glass}}=0.35$ for $\rho_s^*=0.8$). Finally, we note that the glass transition line and the freezing line are notably closer for $\phi_{\mathrm{HS}}^{\mathrm{eff}}$ than for ϕ_{AO}.

We have also computed the nonergodicity parameter $f_{\mathbf{q}}$ at $\eta_b=\eta_b^{\mathrm{glass}}$, for the two potentials in the high ρ_s^* region. The features observed (oscillatory behavior, extension with q) are those already evidenced in the literature for the "repulsive" glass (for ϕ_{AO}) and the "attractive" one (for $\phi_{\mathrm{HS}}^{\mathrm{eff}}$). In the latter case, we checked that the attractive glass is also found for $q=5$. For such moderately asymmetric mixtures, no similar observation has been made up to now from standard modeling of the depletion potential, to the best of our knowledge.

B. Interpretation

Aside from the similarities in the phase diagrams of the OA and HS mixtures that reflect the generic properties of the effective potential (hard-core+short-range depletion induced attraction), we have evidenced above significant differences. Our interpretation of this specificity is based on the fact that the HS depletion potential has a more complex dependence on the physical parameter q and ρ_s^* than the AO one. Indeed, ϕ_{AO} can be written as the product of two independent factors: $\phi^{\mathrm{AO}}(x)=\rho_s^* V_q(x)$ where V_q depends on q but not on ρ_s^* [see Eq. (9)] and operates in the range $1 \leqslant x \leqslant 1+1/q$. In other words, the "intrinsic range" of ϕ_{AO} is determined solely by q, while the factor ρ_s^* simply plays the role of an inverse temperature as with standard potentials such as the Yukawa one. The phase behavior of the AO effective fluid is thus expected to be roughly similar to that found for these potentials. In particular, the stability of the FF binodal, the shape of the FS one, and the existence of an attractive glass should depend only on the value of q. Our results confirm this view. A detailed account of the behavior of the glass transition line for $\rho_s^* > 0.8$ would, however, require a more specific study.

For the binary HS mixture, the structure and dependence with q and ρ_s^* of the depletion potential is more complex. Since $\phi_{\mathrm{HS}}^{\mathrm{eff}}$ is obtained numerically, the influence of these factors is difficult to specify but it can be analyzed from the approximate expression of Götzelmann, Evans, and Dietrich [77]:

$$\phi_{\mathrm{GED}}(x) = \begin{cases} \infty, & x < 1 \\ -\dfrac{3}{2}(q+1)\eta_s^*[q^2x'^2 + \eta_s^*(3qx' + 4q^2x'^2) + 2\eta_s^{*2}(6qx' + 5q^2x'^2)], & 1 \leqslant x \leqslant 1+\dfrac{1}{q} \\ 0, & x > 1+\dfrac{1}{q}, \end{cases} \tag{14'}$$

where $x'=x-1-\frac{1}{q}$ ($\frac{-1}{q} \leqslant x' \leqslant 0$ in the range $1 \leqslant x \leqslant 1+\frac{1}{q}$) and $\eta_s^*=\frac{\pi}{6}\rho_s^*$. This potential, though truncated for $x>1+\frac{1}{q}$, gives a correct description of the binodals (see Sec. IV of Ref. [33] for the FS binodal), and we have checked on a few examples that this also holds for the glass transition line. We see in Eq. (14) that, for a fixed value of q, the "shape" of ϕ_{GED} depends this time on η_s^*. To be more specific, three parameters characterize the variations of ϕ_{GED}: the width δx of the attraction well [Fig. 5(a)], the magnitude $\Delta\phi$ of the repulsive barrier [Fig. 5(b)], and the contact value $\phi_{\mathrm{HS}}^{\mathrm{eff}}(\sigma_b)$ [Fig. 5(c)]. Of course the specific features of the transition lines observed for $\phi_{\mathrm{HS}}^{\mathrm{eff}}$ result from the simultaneous interplay of these three effects that cannot be separated in the analysis.

1. Variation of the width δx

From Eq. (14), one has $\delta x = 1/q[(1-\eta_s^*)(1+2\eta_s^*)/1+4\eta_s^*+10\eta_s^{*2}]$. δx decreases rapidly when η_s^* increases [Fig. 5(a)]: one roughly has $\delta x \approx \delta x_0/4$ for $\eta_s^*=0.4$, where $\delta x_0=\delta x(\eta_s^*=0)$. The width δx can thus be very short, even for moderate q. This explains why the features that are typical of very short-range attractions can be observed for moderate q, as found previously for $q=4$. This has two important consequences: the onset, for sufficient values of η_s^*, of the attractive glass, and the absence of the FF binodal. For the former, a very short attraction range is indeed required. For the condensation of the fluid, it normally takes place when the decrease in potential energy outweighs the entropy loss. This

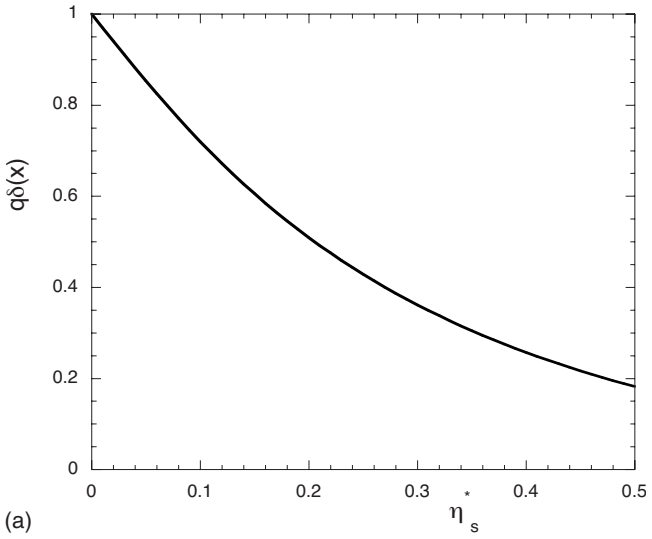

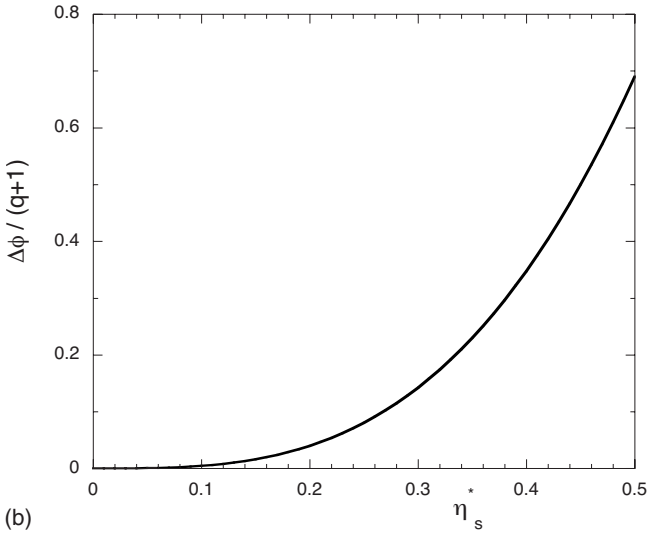

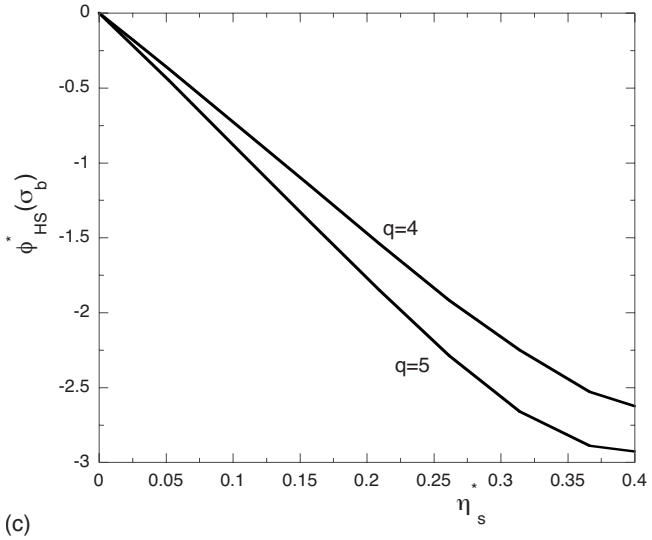

FIG. 5. Variation with η_s^* of the characteristics of the effective potential (HS mixture) for $q=4$. (a) Reduced width of the attraction well; (b) repulsive barrier; (c) contact value. In (a) and (b) GED potential; in (c) RHNC potential.

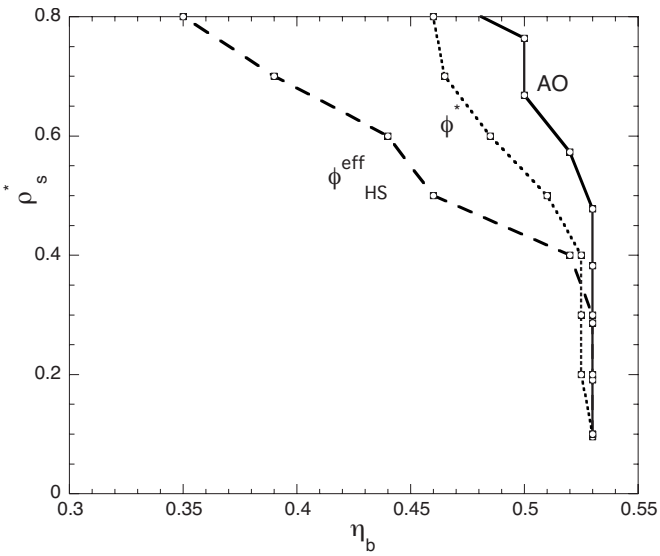

FIG. 6. Glass transition lines of the EOCF for $q=4$, for the Asakura-Oosawa and HS mixture effective potentials and the truncated HS potential ϕ^*.

would correspond here to the high η_s^* region. But as this energy lowering is opposed by a simultaneous decrease of δx in this region (less particles benefit from the attraction), the FF transition is not observed for these values of q.

2. Variation of the barrier $\Delta\phi$

From the expression of the GED potential one gets $\Delta\phi = \frac{27}{8}(q+1)\eta_s^{*3}[(1+4\eta_s^*)^2/1+4\eta_s^*+10\eta_s^{*2}]$. Figure 5(b) shows its strong concavity for $\eta_s^* \leqslant 0.3$. While $\Delta\phi$ is negligible at low η_s^*, it is sizeable for $\eta_s^* \geqslant 0.25$. Its influence on the glass transition line is shown in Fig. 6 for $q=4$: this line is computed with $\phi_{\mathrm{HS}}^{\mathrm{eff}}$ and with its truncated version $[\phi^*(x \leqslant 1+\delta x) = \phi_{\mathrm{HS}}^{\mathrm{eff}}(x),\ \phi^*(x>1+\delta x)=0]$. The line computed with ϕ^* departs strongly from that with the full $\phi_{\mathrm{HS}}^{\mathrm{eff}}$ potential. The attractive glass is generally interpreted as resulting from a trapping effect induced by the short-range attraction between big particles at contact with each other. This trapping is enhanced by the repulsive barrier $\Delta\phi$ when η_s^* is large enough, as this is evidenced on the pdf, $g(r)$, in Fig. 7: with $\phi_{\mathrm{HS}}^{\mathrm{eff}}$, for $q=4$, $\rho_s^*=0.6$, and $\eta_b=0.4$ (that is close to the glass transition line), we see that $g(r)$ drops much below unity right after the depletion well (roughly $r/\sigma_b \geqslant 1.06$ here) while with ϕ^* we have $g(r) \approx 1$.

Note that this result reinforces the analogy already proposed (see Sec. V of Ref. [2]) between the attractive glass and the isostructural SS transitions. Both transitions are indeed observed for very short-range attractive HS, as they involve states in which the particles are very close to each other (for the SS transition, it is the close packing solid). They are further favored by the combination of a narrow attractive well and a repulsive barrier [78]. The difference between the glass transition lines obtained for $\phi_{\mathrm{HS}}^{\mathrm{eff}}$ and ϕ^*—which have exactly the same attractive tail—show that the attraction range is not the unique parameter that determines the existence of the attractive glass.

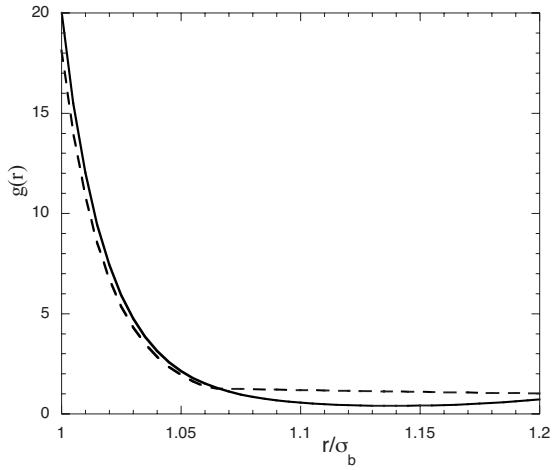

FIG. 7. Pair distribution function near contact of the EOCF computed for $\phi_{\mathrm{HS}}^{\mathrm{eff}}$ (solid line) and ϕ^{*} (dashes) for $q=4$, $\eta_b=0.6$, and $\rho_s^{*}=0.6$.

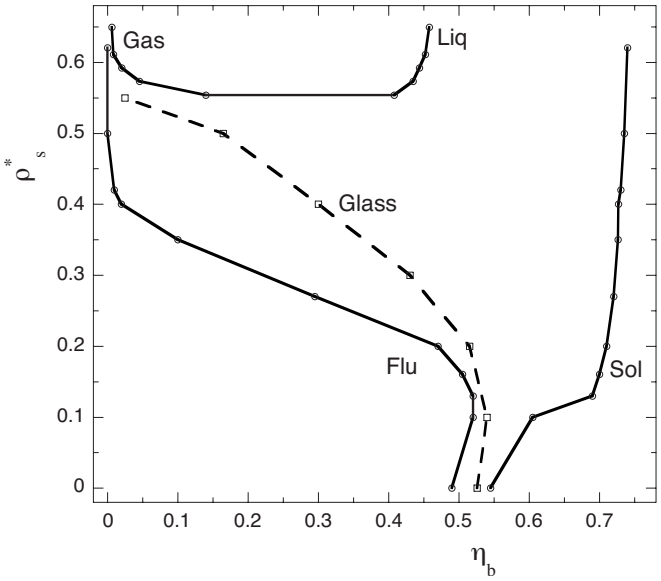

FIG. 8. Phase diagram of the HS mixture for $q=10$ in the EOCF representation. Solid lines, binodals; dashes, glass transition line. The FF binodal is that of the true mixture with η_s^{*} given by the osmotic equilibrium [21].

3. Nonlinearity of $\phi_{\mathrm{HS}}^{\mathrm{eff}}(\sigma_b)$

Another specificity of the HS depletion potential is that its contact value $\phi_{\mathrm{HS}}^{\mathrm{eff}}(\sigma_b)$ does not vary linearly with ρ_s^{*}. This is due to the correlations between the small particles that are neglected in the AO model. We see in Fig. 5(c), for $q=4,5$, that $\phi_{\mathrm{HS}}^{\mathrm{eff}}(\sigma_b)$ increases more and more slowly when ρ_s^{*} is large (it becomes almost constant for $\rho_s^{*}\geqslant 0.7$). This causes first the persistence of the fluid phase up to $\eta_b\approx 0.1$, contrarily to what is observed for the AO potential: indeed, the (negative) energetic gain associated to the close packing solid is not sufficient to induce the total disappearance of the homogeneous fluid phase (see Sec. 4 of Ref. [33] for a discussion of the FS transition based on the free energy landscape). The second consequence of this nonlinearity of $\phi_{\mathrm{HS}}^{\mathrm{eff}}(\sigma_b)$ is that the decrease with ρ_s^{*} of the glass transition critical packing fraction slows down for $\rho_s^{*}>0.6$.

C. HS mixture for $q=10$

We finally complete this study by showing (Fig. 8) the phase diagram of the HS depletion potential including the glass transition line for $q=10$. This size ratio has been extensively studied in the theoretical literature as a prototype of colloidal suspensions (it has been recently used to establish the equivalence of the EOCF and the true mixture in the dense fluid region [21]). The results obtained are similar with those obtained for $q=12.5$, except that the SS transition is not stable.

IV. CONCLUSION

In this paper we have investigated the binodals and the glass transition lines of two models of asymmetric binary mixtures, the Asakura-Oosawa and the HS mixture. The calculations have been done in the effective one-component representation for size ratios corresponding to moderately and strongly asymmetric mixtures. These models are frequently used in the theoretical analysis of certain mixtures of colloids (polymer-colloid, and colloid-colloid) in which depletion effects are expected to be important. Nevertheless, their complete phase diagram has not been presented yet, despite the importance of considering both equilibrium and nonequilibrium states. It appears that in the strong asymmetry regime (say $q\geqslant 10$), the two models behave quite similarly. Their phase diagram shows the characteristic features expected for extremely short-range attractive potentials—here the depletion potential: in particular, the existence within the broad fluid-solid coexistence domain of an attractive glass at low packing fraction, which preempts the metastable gas-liquid transition. By including the glass transition, we confirm here that the differences between the two models are truly weak for these size ratios. The situation is different at moderate size asymmetry (e.g., $q=4$). While the phase behavior of the Asakura-Oosawa model follows indeed the predictions for moderately short-range attractions (say for the Yukawa potential with $\kappa^{*}=7$), the HS mixture model shows a more specific behavior. Of course, some important differences, such as the absence of a fluid-fluid binodal, have already been pointed out in the literature. Our results show that unexpected features can also be observed concerning the glass transition. Indeed, an attractive glass is also observed in a significant domain of big spheres packing fraction; up to now, this feature was expected only for highly asymmetric mixtures. These results can be understood from the characteristics of the HS depletion potential whose shape and variation with the size ratio and the solvent density are more complex than those of the Asakura-Oosawa potential. In particular, other characteristics than the sole attraction range may have a significant role. In real suspensions, many additional interactions should, of course, be considered. One may thus expect the effective potential between the big particles to have in most cases a degree of complexity which, like the HS depletion potential, cannot be reduced to those of the standard ones used in the theory of simple fluids. This issue

has already been raised in several studies of equilibrium states and it is confirmed experimentally. Indeed, the experimental phase diagram of a mixture of two supposedly HS silica particles with different sizes ($q=9.3$) [30] shows significant differences with the binary HS mixture model, at least from a quantitative point of view (enlargement of the FS binodal, location with respect to the glass transition line). From a theoretical point of view, it was already shown that pseudobinary mixtures of supposedly "hard-sphere-like" colloids could in fact behave differently when compared to mixtures of true hard spheres [33], as far as the binodals are concerned. For the glass transition now, more refined modeling, including small additions to the hard-core interaction, might equally reveal original behaviors, such as, for example, the existence of an attractive glass in the homogeneous fluid region. Work in this direction is in progress.

APPENDIX

In the AO mixture, the interactions between small particles are neglected. The small particle density in the reservoir is thus related to the chemical potential μ_s by $\rho_s^r = \frac{\exp(\beta\mu_s)}{\Lambda_s^3}$ (perfect gas). The density ρ_s in the mixture is given by

$$\rho_s = \frac{1}{V}\frac{\partial F}{\partial \mu_s} \tag{A1}$$

where $F=-k\,T\,Ln(Z)$ is given by Eqs. (1) and (2). The partition function Z can be expressed as a sum over the big particle configurations

$$Z = \frac{1}{N_b!\Lambda_b^{3N_b}} \int dR_b^{N_b} e^{-\beta H_{bb}} \left| \sum_{N_s} \frac{e^{\beta\mu_s N_s}}{N_s!\Lambda_s^{3N_s}} \int dr_s^{N_s} e^{-\beta H_{sb}} \right|. \tag{A2}$$

H_{bb} and H_{sb} are, respectively, the big-big and small-big particle interaction Hamiltonian ($H_{ss}=0$). As the interactions are pure HS ones, one has

$$e^{-\beta H_{bb}} e^{-\beta H_{sb}} = \begin{cases} 1 & \text{(allowed configuration)} \\ 0 & \text{(forbidden one).th} \end{cases} \tag{A3}$$

Furthermore, with $H_{ss}=0$, one has

$$\int dr_s^{N_s} e^{-\beta H_{sb}} = \left(\int dr_s e^{-\beta H_{sb}} \right)^{N_s}. \tag{A4}$$

From (A3) and (A4), Z can be written as

$$Z = \frac{1}{N_b!\Lambda_b^{3N_b}} \int_{\Omega'} dR_b^{N_b} \left| \sum_{N_s} \frac{(e^{\beta\mu_s} V(R^{N_b}))^{N_s}}{\Lambda_s^{3N_s} N_s!} \right|, \tag{A5}$$

where Ω' is the $3N_b$-dimensional volume of the allowed configurations of the big particles, in the absence of the small ones, and $V(R_b^{N_b})$ the (three-dimensional) free volume for one small particle once the N_b big ones are fixed. Equation (A5) can be written as

$$Z = \frac{1}{N_b!\Lambda_b^{3N_b}} \int_{\Omega'} dR^{N_b} \exp[\rho_s^r V(R^{N_b})]. \tag{A6}$$

$V(R_b^{N_b})$ is a bonded function of $\{\mathbf{R}^{N_b}\}: V_{\min} \leqslant V(\mathbf{R}^{N_b}) \leqslant V_{\max}$ (the expressions of $V_{\min}$ and $V_{\max}$ are given below). It can be written as $V(\mathbf{R}^{N_b}) = V_m + \Delta V(\mathbf{R}^{N_b})$, where V_m will be chosen successively as $V_m = V_{\min}$ $[\Delta V(R_b^{N_b}) \geqslant 0]$, and $V_m = V_{\max}$ $[\Delta V(R_b^{N_b}) \leqslant 0]$. Equation (A6) can be written as

$$Z = \frac{1}{N_b!\Lambda_b^{3N_b}} \exp(\rho_s^r V_m) \int_{\Omega'} dR^{N_b} \exp[\rho_s^r \Delta V(R^{N_b})]. \tag{A7}$$

From Eqs. (A1) and (A2) and Eq. (A7), one gets

$$\rho_s = \frac{V_m}{V}\rho_s^r + \Delta\rho_s \tag{A8}$$

with

$$\Delta\rho_s = \frac{1}{\beta V}\frac{\partial}{\partial\mu_s}\left\{ Ln\left(\int d\mathbf{R}^{N_b} \exp[\rho_s^r \Delta V(\mathbf{R}^{N_b})] \right) \right\}. \tag{A9}$$

One has thus

$$\Delta\rho_s = \frac{1}{\beta V}\frac{\partial\rho_s^r}{\partial\mu_s} \frac{\int d\mathbf{R}^{N_b} \Delta V(\mathbf{R}^{N_b}) \exp[\rho_s^r \Delta V(\mathbf{R}^{N_b})]}{\int d\mathbf{R}^{N_b} \exp[\rho_s^r \Delta V(\mathbf{R}^{N_b})]}. \tag{A10}$$

The sign of $\Delta\rho_s$ is that of the denominator in Eq. (A10). For $V_m = V_{\min}$ (respectively, $V_m = V_{\max}$), $\Delta V(\mathbf{R}^{N_b})$ is a positive (respectively, negative) function of $\{\mathbf{R}^{N_b}\}$, and thus $\Delta\rho_s > 0$ (respectively, $\Delta\rho_s < 0$). This leads to

$$\frac{V_{\min}}{V}\rho_s^r < \rho_s < \frac{V_{\max}}{V}\rho_s^r. \tag{A11}$$

Now, $V_{\min}$ and $V_{\max}$ can be deduced from the following considerations: $V(R_b^{N_b}) = V - V_{\text{exc}}$, where V_{exc} is the volume that is forbidden to a small particle, due to the big ones. It is maximum when the exclusion volumes, $V_0 = (4\pi\sigma_{sb}^3/3)$, due to each big sphere, do not overlap. $V_{\text{exc}}^{\max} = N_b V_0$, and thus

$$V_{\min} = V\left(1 - \frac{4\pi\rho_b\sigma_{sb}^3}{3}\right). \tag{A12}$$

The minimum value of V_{exc} corresponds to the configurations for which the overlap of these exclusion volumes is maximum. This is realized by the close packing solid configurations, for which the overlap volume per big particle is

$$V_{\text{over}} = \frac{z}{2} V_1,$$

$$V_1 = 2\pi\sigma_{sb}^3 \left(\frac{1}{(q+1)^2} - \frac{1}{3(q+1)^3} \right), \tag{A13}$$

where $z=12$ is the number of nearest neighbors. The expression (A13) of V_1 is that leading to the potential of Asakura and Oosawa [4,5]. Finally, Eqs. (A8), (A12), and (A13) lead to

$$1 - \frac{4\pi}{3}\rho_b\sigma_{sb}^3 < 1 - \frac{\rho_s}{\rho_s^r} < 1 - \frac{4\pi}{3}\rho_b\sigma_{sb}^3 \left(1 - \frac{9}{(q+1)^2} + \frac{3}{(q+1)^3} \right). \tag{A14}$$

The difference $\frac{\delta\rho_s}{\rho_s^r}$ between the maximum and minimum value of $\frac{\rho_s}{\rho_s^r}$ is given by

$$\frac{\delta\rho_s}{\rho_s^r} < 4\pi\rho_b\sigma_{sb}^3 \left(\frac{3}{(q+1)^2} + \frac{1}{(q+1)^3} \right), \tag{A15}$$

which scales as $\frac{\delta\rho_s}{\rho_s^r} \approx \frac{9\eta_b}{q^2}$ for $q \gg 1$.

[1] A. Yethiraj and A. van Blaaderen, Nature (London) **421**, 513 (2003).
[2] G. Foffi, G. D. McCullagh, A. Lawlor, E. Zaccarelli, K. A. Dawson, F. Sciortino, P. Tartaglia, D. Pini, and G. Stell, Phys. Rev. E **65**, 031407 (2002).
[3] N. M. Dixit and C. F. Zukoski, Phys. Rev. E **67**, 061501 (2003).
[4] S. Asakura and F. Oosawa, J. Chem. Phys. **22**, 1255 (1954).
[5] A. Vrij, Pure Appl. Chem. **48**, 471 (1976).
[6] J. L. Lebowitz and S. Rowlinson, J. Chem. Phys. **41**, 133 (1964).
[7] T. Biben and J. P. Hansen, Phys. Rev. Lett. **66**, 2215 (1991).
[8] H. N. W. Lekkerkerker, W. C. K. Poon, N. Pusey, A. Stroobants, and P. B. Warren, Europhys. Lett. **20**, 559 (1992); H. N. W. Lekkerkerker and A. Stroobants, Physica A **195**, 387 (1993).
[9] Y. Rosenfeld, Phys. Rev. Lett. **72**, 3831 (1994).
[10] S. Amokrane and C. Regnaut, Phys. Rev. E **53**, 1990 (1996).
[11] C. Caccamo and G. Pellicane, Physica A **235**, 149 (1997).
[12] M. Dijkstra, R. Roij, and R. Evans, Phys. Rev. Lett. **81**, 2268 (1998); **82**, 117 (1999); Phys. Rev. E **59**, 5744 (1999).
[13] N. G. Almarza and E. Enciso, Phys. Rev. E **59**, 4426 (1999).
[14] E. Velasco, G. Navascuès, and L. Mederos, Phys. Rev. E **60**, 3158 (1999).
[15] M. Dijkstra, J. M. Brader, and R. Evans, J. Phys.: Condens. Matter **11**, 10079 (1999).
[16] J. Clement-Cottuz, S. Amokrane, and C. Regnaut, Phys. Rev. E **61**, 1692 (2000).
[17] R. Roth, R. Evans, and S. Dietrich, Phys. Rev. E **62**, 5360 (2000).
[18] H. N. W. Lekkerkerker and S. M. Oversteegen, J. Phys.: Condens. Matter **14**, 9317 (2002).
[19] W. C. K. Poon, J. Phys.: Condens. Matter **14**, R859 (2002).
[20] D. Fu, Y. Li, and J. Wu, Phys. Rev. A **68**, 011403 (2003).
[21] A. Ayadim and S. Amokrane, Phys. Rev. E **74**, 021106 (2006).
[22] G. Jackson, J. S. Rowlinson, and F. van Swol, J. Phys. Chem. **91**, 4907 (1987).
[23] T. Biben, P. Bladon, and D. Frenkel, J. Phys.: Condens. Matter **8**, 10799 (1996).
[24] C. Dress and W. Krauth, J. Phys. A **28**, L597 (1995); A. Buhot and W. Krauth, Phys. Rev. Lett. **80**, 3787 (1998).
[25] L. Lue and L. V. Woodcock, Mol. Phys. **96**, 143 (1999).
[26] J.-G. Malherbe and S. Amokrane, Mol. Phys. **99**, 355 (2001); S. Amokrane, A. Ayadim, and J. G. Malherbe, J. Phys.: Condens. Matter **15**, S3443 (2003).
[27] S. Amokrane, A. Ayadim, and J. G. Malherbe, J. Chem. Phys. **123**, 174508 (2005).
[28] J. S. van Duijneveldt, A. W. Heinen, and H. N. W. Lekkerkerker, Europhys. Lett. **21**, 369 (1993).
[29] P. D. Kaplan, J. L. Rouke, A. G. Yodh, and D. J. Pine, Phys. Rev. Lett. **72**, 582 (1994).
[30] A. Imhof and J. K. G. Dhont, Phys. Rev. Lett. **75**, 1662 (1995); Phys. Rev. E **52**, 6344 (1995).
[31] A. D. Dinsmore, A. G. Yodh, and D. J. Pine, Phys. Rev. E **52**, 4045 (1995).
[32] P. G. Bolhuis, A. A. Louis, and J-P. Hansen, Phys. Rev. Lett. **89**, 128302 (2002).
[33] Ph. Germain, J. G. Malherbe, and S. Amokrane, Phys. Rev. E **70**, 041409 (2004).
[34] P. Bolhuis, M. Hagen, and D. Frenkel, Phys. Rev. E **50**, 4880 (1994).
[35] M. Hasegawa, J. Chem. Phys. **108**, 208 (1998).
[36] W. Götze, in *Liquids, Freezing and Glass Transition*, edited by J-P. Hansen, D. Levesque, and J. Zinn-Justin (North-Holland, Amsterdam, 1991), pp. 287–50.
[37] K. A. Dawson, Curr. Opin. Colloid Interface Sci. **7**, 218 (2002).
[38] E. Bartsch, V. Frenz, J. Baschnagel, W. Schärtl, and H. Silescu, J. Phys.: Condens. Matter **106**, 3743 (1996).
[39] T. Eckert and E. Bartsch, Phys. Rev. Lett. **89**, 125701 (2002).
[40] K. N. Pham *et al.*, Science **296**, 104 (2002); K. N. Pham, S. U. Egelhaaf, P. N. Pusey, and W. C. K. Poon, Phys. Rev. E **69**, 011503 (2004).
[41] W. C. K. Poon, K. N. Pham, S. U. Egelhaaf, and P. N. Pusey, J. Phys.: Condens. Matter **15**, S269 (2003).
[42] S. A. Shah, Y.-L. Chen, K. S. Schweizer, and C. F. Zukoski, J. Chem. Phys. **119**, 8747 (2003).
[43] S. Manley, H. M. Wyss, K. Miyazaki, J. C. Conrad, V. Trappe, L. J. Kaufman, D. R. Reichman, and D. A. Weitz, Phys. Rev. Lett. **95**, 238302 (2005).
[44] L. J. Kaufman and D. A. Weitz, J. Chem. Phys. **125**, 074716 (2006).

[45] P. N. Pusey and W. van Megen, Phys. Rev. Lett. **59**, 2083 (1987).
[46] W. van Megen and P. N. Pusey, Phys. Rev. A **43**, 5429 (1991).
[47] W. van Megen and S. M. Underwood, Phys. Rev. E **49**, 4206 (1994).
[48] U. Bengtzelius, W. Götze, and A. Sjölander, J. Phys. C **17**, 5915 (1984).
[49] W. Götze and L. Sjögren, Phys. Rev. A **43**, 5442 (1991); Rep. Prog. Phys. **55**, 241 (1992).
[50] W. van Megen and S. M. Underwood, Phys. Rev. Lett. **70**, 2766 (1993).
[51] J. Bergenholtz and M. Fuchs, Phys. Rev. E **59**, 5706 (1999); J. Phys.: Condens. Matter **11**, 10171 (1999).
[52] L. Fabbian, W. Götze, F. Sciortino, P. Tartaglia, and F. Thiery, Phys. Rev. E **59**, R1347 (1999); **60**, 2430 (1999).
[53] K. Dawson, G. Foffi, M. Fuchs, W. Götze, F. Sciortino, M. Sperl, P. Tartaglia, Th. Voigtmann, and E. Zaccarelli, Phys. Rev. E **63**, 011401 (2000).
[54] E. Zaccarelli, G. Foffi, K. A. Dawson, F. Sciortino, and P. Tartaglia, Phys. Rev. E **63**, 031501 (2001).
[55] G. Foffi, K. A. Dawson, S. V. Buldyrev, F. Sciortino, E. Zaccarelli, and P. Tartaglia, Phys. Rev. E **65**, 050802(R) (2002); E. Zaccarelli, G. Foffi, K. A. Dawson, S. V. Buldyrev, F. Sciortino, and P. Tartaglia, *ibid.* **66**, 041402 (2002); F. Sciortino, P. Tartaglia, and E. Zaccarelli, Phys. Rev. Lett. **91**, 268301 (2003).
[56] G. Foffi, C. De Michele, F. Sciortino, and P. Tartaglia, J. Chem. Phys. **122**, 224903 (2005).
[57] E. Zaccarelli, H. Löwen, P. P. F. Wessels, F. Sciortino, P. Tartaglia, and C. N. Likos, Phys. Rev. Lett. **92**, 225703 (2004).
[58] M. Fuchs and K. S. Schweizer, J. Phys.: Condens. Matter **14**, R239 (2002).
[59] M. J. Greenall and Th. Voigtmann, J. Chem. Phys. **125**, 194511 (2006).
[60] T. L. Hill, *Statistical Mechanics* (Dover, New York, 1987).
[61] J. P. Hansen and I. R. McDonald, *Theory of Simple Liquids* (Academic, New York, 1986).
[62] A. J. Archer and R. Evans, J. Chem. Phys. **118**, 9726 (2003).
[63] F. Lado, S. M. Foiles, and N. W. Ashcroft, Phys. Rev. A **28**, 2374 (1983).
[64] Y. Rosenfeld, J. Chem. Phys. **98**, 8126 (1993).
[65] S. Amokrane and J. G. Malherbe, J. Phys.: Condens. Matter **13**, 7199 (2001); **14**, 3845(E) (2002).
[66] H. Shinto, M. Miyahara, and K. Higashitani, J. Colloid Interface Sci. **209**, 79 (1999).
[67] J. G. Malherbe, C. Regnaut, and S. Amokrane, Phys. Rev. E **66**, 061404 (2002).
[68] A. Malijevsky and S. Labik, Mol. Phys. **60**, 663 (1987); S. Labik and A. Malijevski, *ibid.* **67**, 431 (1989).
[69] P. Germain and S. Amokrane, Phys. Rev. E **65**, 031109 (2002).
[70] P. N. Pusey, in *Liquids, Freezing and Glass Transition*, edited by J.-P. Hansen, D. Levesque, and J. Zinn-Justin (North-Holland, Amsterdam, 1991), pp. 765–942.
[71] G. Szamel and H. Löwen, Phys. Rev. A **44**, 8215 (1995).
[72] K. Kawasaki, Physica A **208**, 35 (1994).
[73] W. Götze and L. Sjögren, J. Math. Anal. Appl. **195**, 230 (1995).
[74] G. A. Vliegenthart and P. van der Schoot, Europhys. Lett. **62**, 600 (2003).
[75] N. Kikuchi and J. Horbach, Europhys. Lett. **77**, 26001 (2007).
[76] M. Schmidt, H. Lowen, J. M. Brader, and R. Evans, Phys. Rev. Lett. **85**, 1934 (2000); J. Phys.: Condens. Matter **14**, 9353 (2002).
[77] B. Götzelmann, R. Evans, and S. Dietrich, Phys. Rev. E **57**, 6785 (1998).
[78] A. R. Denton and H. Löwen, J. Phys.: Condens. Matter **9**, 8907 (1997).